ResearchGate

See discussions, stats, and author profiles for this publication at: https://www.researchgate.net/publication/236851384

Synthesis, spectroscopic properties, and stabilities of ternary europium complex in SBA-15 and periodic mesoporous organosilica: A comparative study

ARTICLE *in* THE JOURNAL OF PHYSICAL CHEMISTRY C · JANUARY 2009

Impact Factor: 4.77

CITATION
1

READS
23

4 AUTHORS, INCLUDING:

Xianmin Guo
Changchun Normal University
31 PUBLICATIONS **786** CITATIONS
SEE PROFILE

Lianshe Fu
University of Aveiro
124 PUBLICATIONS **2,422** CITATIONS
SEE PROFILE

Available from: Lianshe Fu
Retrieved on: 23 January 2016

Synthesis, Spectroscopic Properties, and Stabilities of Ternary Europium Complex in SBA-15 and Periodic Mesoporous Organosilica: A Comparative Study

Xianmin Guo,[†,‡] Huadong Guo,[†,‡] Lianshe Fu,[§] Ruiping Deng,[†] Wan Chen,[†,‡] Jing Feng,[†,‡] Song Dang,[†,‡] and Hongjie Zhang*[,†]

State Key Laboratory of Rare Earth Resource Utilizations, Changchun Institute of Applied Chemistry, Chinese Academy of Sciences, 5625 Renmin Street, Changchun 130022, P. R. China, Graduate School of the Chinese Academy of Sciences, P. R. China, and Department of Physics, CICECO, University of Aveiro, 3810-193 Aveiro, Portugal

Received: October 29, 2008; Revised Manuscript Received: December 11, 2008

Ternary europium complex $Eu(tta)_3phen$ was covalently bonded with the general mesoporous material SBA-15 and SBA-15-type of periodic mesoporous organosilica (PMO) material via impregnation of $Eu(tta)_3 \cdot 2H_2O$ into phen-S15 and phen-PMO, respectively, through a ligand exchange reaction. The parent materials of phen-S15 and phen-PMO were synthesized by co-condensation of tetraethylorthosilicate (TEOS) or 1,2-bis(triethoxysilyl)ethane (BTESE) and the functionalized chelate ligand 5-(*N*,*N*-bis(3-triethoxysilyl)propyl)ureyl-1,10-phenanthroline (phen-Si) in the presence of Pluronic P123 surfactant as template, which were confirmed by SEM, XRD, FTIR, ^{29}Si CP-MAS NMR, and N_2 adsorption measurements. The photophysical properties of the hybrids, such as the photoluminescence (PL) spectra, PL intensities, symmetry properties, luminescence decay times, and Judd−Ofelt parameters, were investigated in detail. Compared to the sample of $Eu(tta)_3phen$-PMO, the mesoporous hybrid material $Eu(tta)_3phen$-S15 exhibited longer luminescent decay time and higher luminescence intensity, emission quantum efficiency (q), and absolute quantum yield (Φ), which were quantitatively stressed by the emission spectra and the calculated values of q of Eu^{3+} ion. Meanwhile, the result of thermal treatment demonstrated that the europium complex in $Eu(tta)_3phen$-S15 material possessed a better thermal stability than that in $Eu(tta)_3phen$-PMO. The above photoluminescence and thermal stability features indicated that SBA-15 is a better host material for lanthanide complex than SBA-15-type PMO material.

Introduction

As well-known, lanthanide (Ln^{3+}) complexes are a very useful and important class of luminescent materials, which have a variety of potential technological applications, such as in fluoroimmunoassays, spectroscopic structural probes in biologically important systems, lasers, optical amplification, light-conversion molecular devices (LCMDs), and organic light-emitting diodes (OLEDs).[1−5] In fact, the photoluminescence of lanthanide complexes must suffer from a process that the coordinated ligands efficiently absorb and transfer light to the luminescent central lanthanide ions (the so-called "antenna effect") because the lanthanide ions are symmetry-forbidden f−f transitions.[6] However, lanthanide complexes have been excluded so far from practical applications essentially due to some disadvantages, such as their low chemical, optical, and thermal stabilities.[7] Since these photophysical properties could be modified by interaction with the host matrix, an investigation on the luminescence properties of lanthanide complexes supported on the inert host matrices has been extensively carried out on, for example, silica-based materials,[8−13] polymers,[14−18] or liquid crystals,[19] forming "organic−inorganic hybrid materials". Among the above host matrices, the mesoporous molecular sieves (MMSs) used as a support for lanthanide complexes have attracted particular attention since they offer many novel and unique properties, such as the rigidity, photostability, and well-defined hydrophilic/hydrophobic phase separation allowing for more sophisticated tuning of the lanthanide complex microenvironment. In the past few years, several research groups incorporated different lanthanide complexes into the channels of the mesoporous materials via simple physical doping or covalent bond grafting techniques.[20−24] Meanwhile, our group has also paid attention to the modification of the mesoporous materials with different lanthanide complexes, including visible (Vis) and near-infrared (NIR) luminescence of Ln^{3+} ions.[25] The results revealed that the obtained materials possessed good luminescent properties and photo- or thermal stabilities.

However, recently much fascinating interest has been devolved to the synthesis of the periodic mesoporous organosilica (PMO) materials (PMOs) in the mesoporous material field, which were reported by three different independently working research groups at the end of the twentieth century.[26] The results of investigation demonstrated that in contrast with the general MMSs, PMOs present better aging and hydrothermal and mechanical stabilities as well as a uniform distribution of organic and inorganic moieties at the molecular level within the framework.[27] These properties open a wide range of novel and exciting opportunities for designing materials and make them more promising as candidates in the fields of advanced catalysis, adsorption, and so on. Moreover, the functionalization for the surfaces of PMOs with organic groups has been widely investigated because surface modification permits tailoring of the surface properties for meeting the numerous potential applications.

* To whom correspondence should be addressed. Fax: +86-431-85698041. E-mail: hongjie@ciac.jl.cn.
† Changchun Institute of Applied Chemistry, Chinese Academy of Sciences.
‡ Graduate School of the Chinese Academy of Sciences.
§ University of Aveiro.

10.1021/jp8095488 CCC: $40.75 © 2009 American Chemical Society
Published on Web 01/20/2009

SCHEME 1: Predicted Structure of the Resulting Hybrid Materials Eu(tta)$_3$phen-S15 (a) and Eu(tta)$_3$phen-PMO (b)

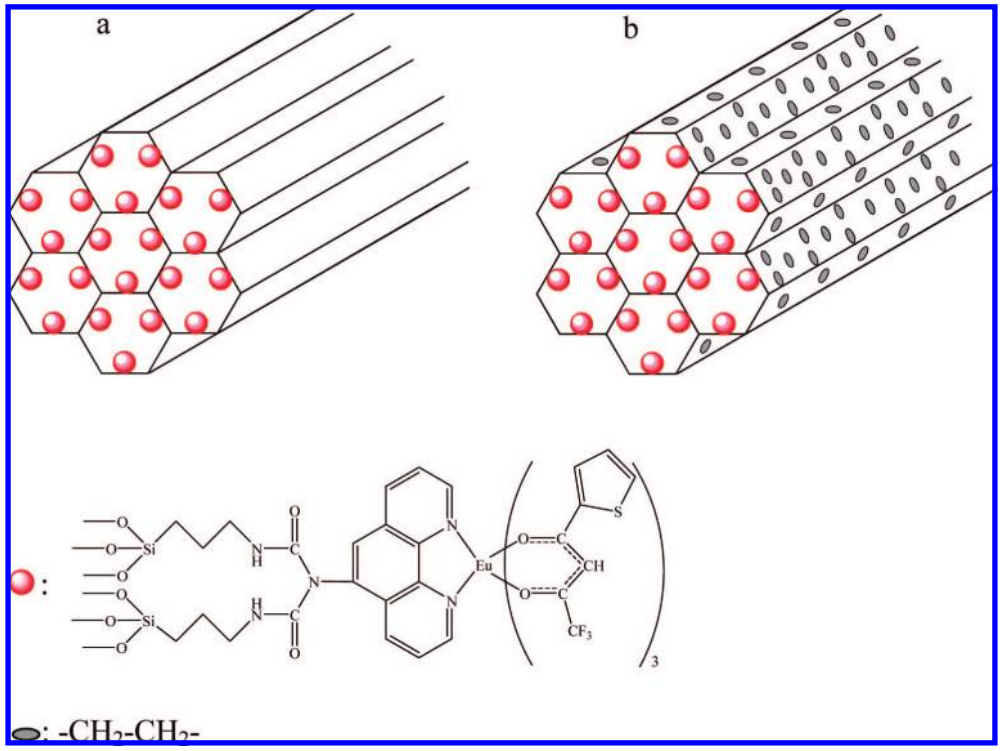

Up to now, the study of the properties of PMOs has mainly focused on the catalysis, adsorption, bioencapsulation, and photoresponsiveness based on the organic molecules.[28−31] However, to the best of our knowledge, the luminescence of lanthanide complex supported on the functionalized PMOs has been rarely reported so far. In this manuscript, we extended our previous approach and synthesized the luminescent PMO material covalently bonded with a ternary lanthanide complex Eu(tta)$_3$phen (tta = 2-thenoyltrifluoroacetonate), designated as Eu(tta)$_3$phen-PMO. In addition, we prepared the generally luminescent mesoporous hybrid material Eu(tta)$_3$phen-S15. Full characterization and detailed studies on the properties of both materials were investigated and compared. The aim of this work is to compare the photoluminescence and thermal stability properties of both samples and to find a suitable candidate host for the lanthanide complexes.

Experimental Section

Materials. 1,2-Bis(triethoxysilyl)ethane (BTESE, Aldrich), 3-(triethoxysilyl)propyl isocyanate (ICPTES, Fluka), triblock copolymer poly(ethylene glyco)-*block*-poly(propylene glycol)-*block*-poly-(ethylene glycol) (Pluronic P123, $EO_{20}PO_{70}EO_{20}$, Aldrich), fuming nitric acid (HNO_3), and ethanol (EtOH) were used as received. The solvent chloroform ($CHCl_3$) was used after desiccation with anhydrous calcium chloride. Europium chloride ($EuCl_3$) was obtained by dissolving Eu_2O_3 (99.99%, Shanghai Yuelong, China) in hydrochloric acid, and the resultant product was dissolved in EtOH to get its solution. The molar concentration of $EuCl_3$ was determined by titration with the standard ethylenediaminetetraacetic acid (EDTA) aqueous solution using hexamethylenetetramine as a buffer agent and xylenol as an indicator. 1,10-Phenanthroline monohydrate (phen, AR) and 2-thenoyltrifluoroacetonate (tta, AR) were bought from Beijing Fine Chemical Co. (Beijing, China).

Synthesis of Phen-Functionalized SBA-15 Mesoporous Material (phen-S15). The starting reagent 5-amino-1,10-phenanthroline (denoted as phen-NH_2) was synthesized according to the procedure described in the literature.[32] The modified phenanthroline 5-(*N*,*N*-bis(3-triethoxysilyl)propyl)-ureyl-1,10-phenanthroline (phen-Si) was prepared by the reaction of phen-NH_2 and ICPTES in $CHCl_3$ as described in ref 33. The phen-SBA-15 was synthesized mainly as described in the literature.[34] Typically, 0.5 g of P123 and 3.17 g of KCl were dissolved in 3.75 g of deionized water and 15 g of 2 M HCl solution at 35 °C under vigorous stirring. A mixture (4.82 mmol) of TEOS and phen-Si was added into the above solution, which was further stirred at 35 °C for 24 h and transferred into a Teflon bottle sealed in an autoclave, which was then heated at 100 °C for 24 h. The solid product was recovered by filtration, washed thoroughly with deionized water, and air-dried at room temperature. Removal of copolymer surfactant P123 was conducted by Soxhlet extraction with ethanol for 24 h to obtain the sample, which was denoted as phen-S15.

Synthesis of Phen-Functionalized PMO Material (phen-PMO). The synthesis procedure of phen-PMO was similar to that of phen-S15 except that TEOS was replaced by BTESE.

Synthesis of SBA-15 Mesoporous Silica Material Covalently Bonded with Ternary Complex Eu(tta)$_3$phen (Eu(tta)$_3$phen-S15). Eu(tta)$_3\cdot 2H_2O$ was prepared by the method described in literature.[8] Eu(tta)$_3$phen-S15 was synthesized according to the literature that we have published before.[25c] The sample was dried at 60 °C under vacuum overnight.

Synthesis of PMO Material Covalently Bonded with Ternary Complex Eu(tta)$_3$phen (Eu(tta)$_3$phen-PMO). The synthesis procedure of Eu(tta)$_3$phen-PMO was similar to that of Eu(tta)$_3$phen-S15 except that phen-S15 was replaced by phen-PMO. The possible structures for both hybrids are shown in Scheme 1.

Characterization. Small-angle X-ray diffraction patterns (XRD) were recorded with Rigaku-Dmax 2500 diffractometer using Cu Kα radiation (40 kV, 200 mA) at a step width of 0.02°. Fourier transform infrared (FTIR) spectra were measured on a Bruker Vertex 70 spectrophotometer within the 4000−400 cm^{-1} wavenumber range at a resolution of 4 cm^{-1} with the KBr pellet

technique. Solid-state ^{29}Si MAS NMR spectra were recorded at 79.46 MHz using a Bruker Avance 400 spectrometer. The chemical shifts were quoted in ppm from tetramethylsilane (TMS). Transmission electron microscopy (TEM) observation was made on a Hitachi H-8110 at an acceleration voltage of 200 kV. Nitrogen (N_2) adsorption−desorption isotherms were measured by using a Nova l000 analyzer with nitrogen. The samples were outgassed for 4 h at 120 °C before the measurements. Surface areas were calculated by the Brunauer−Emmett−Teller (BET) method and pore sizes by the Barrett−Joyner−Halenda (BJH) methods. The fluorescence excitation and emission spectra were recorded on a JY FL-3 spectrophotometer equipped with a 450 W xenon lamp as an excitation source. The luminescence decay times were measured with a Lecroy Wave Runner 6100 Digital Oscilloscope (1 GHz) using different wavenumber lasers (pulse width = 4 ns) as the excitation source (Continuum Sunlite OPO).

Results and Discussion

Phen-Functionalized Parent Materials (Phen-PMO and Phen-S15). Although MCM-41 was discovered in the early 1990s,[35] the development of MMSs revealed that as a host material for lanthanide complexes, SBA-15 appears more attractive than mesoporous silicas M41S. This is due to its much larger uniform pore size and specific area, thicker silica wall, and better stability.[36] As is well-known, the larger pore size and specific surface area make it a fascinating matrix for the insertion of large amounts of bulky molecules with functional properties, and the better stability makes it very suitable for immobilization of functional molecules, which are propitious for improvement of the content, luminescent properties, and thermal stabilities of lanthanide complexes. In addition, because of the unique concentration effect of lanthanide complexes, the lanthanide ions had better be dispersed uniformly in the surface of mesoporous materials at a molecular level since the high doping content of lanthanide ion usually quenches the luminescence. The co-condensation method enables a high and homogeneous surface coverage of organosilane functionalities. Therefore, we focused on the synthesis of the type of SBA-15 mesoporous materials via the co-condensation method in this paper. Meanwhile, the concentration effect of phen-Si on the pore structure should also be considered since the high loading of functionality will result in the reduction of diffraction intensity or the disordered structure for SBA-15-type materials, while the low loading of functionality will be followed with a relatively decreasing amount of the lanthanide complexes linked to the functionalized frameworks, leading to the reduction of their luminescent intensities. According to our previous report,[25c] an optimum molar ratio (phen-Si/(phen-Si + TEOS) = 0.04) can be employed to synthesize phen-functionalized SBA-15 with a high loading of functionality yet a good mesostructure. Thus, the molar ratio of 0.04 is used for the preparation of phen-S15 and phen-PMO, respectively.

The microscopic morphologies of surfactant-extracted phen-S15 and phen-PMO materials are clearly observed in SEM images (see Figure 1). Two kinds of materials present uniformly unique bundles, which are composed of pearl chainlike arrays via self-assembly. Meanwhile, each pearl chainlike array consists of many hexagonal disks with a diameter of about 500 nm and a length of about 400 nm. However, the external surface of phen-PMO seems to be rougher than that of phen-S15, which is perhaps due to the coexistence of organic and inorganic groups on the surface.

Figure 2 exhibits the XRD patterns of surfactant-extracted phen-S15 and phen-PMO materials. It can be seen that both

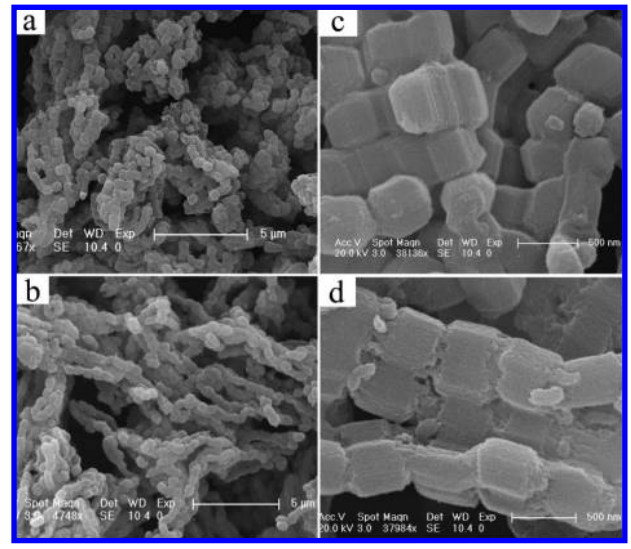

Figure 1. SEM images of surfactant-extracted phen-S15 (a), phen-PMO (b), and corresponding magnified images (c) and (d).

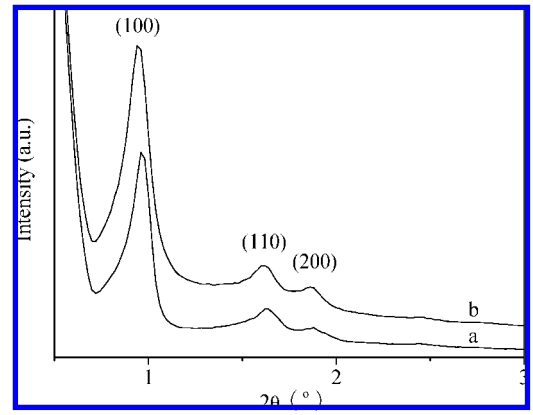

Figure 2. XRD patterns for surfactant-extracted phen-S15 (a) and phen-PMO (b).

samples exhibit three well-resolved diffraction peaks in the 2θ range of 0.5−2°, which are indexed as the (100), (110), and (200) diffractions, respectively, characteristic of SBA-15-type two-dimensional hexagonal (*P6mm*).[36] This observation indicates that the highly ordered mesostructures of SBA-15-type were obtained with the molar ratio of 0.04. At the same time, the corresponding unit cell parameters a ($a = d_{hkl}/(h^2 + k^2 + l^2)^{1/2}$) of phen-S15 and phen-PMO materials were calculated and are listed in Table 1.

In order to further investigate the channel structure of phen-S15 and phen-PMO materials, the characterization of the nitrogen adsorption−desorption was also carried out. The corresponding isotherms are displayed in Figure 3. Both materials exhibit the type-IV isotherm curves with H^1-type hysteresis loops at high relative pressure, typical of conventional mesoporous material employing this kind of surfactant.[36] The pore diameters (d), specific surface areas (S_{BET}), and pore volume (V) of these samples were calculated by the BJH method, and the results are also summarized in Table 1. From d, S_{BET}, and V of phen-S15 and phen-PMO, it is worth noting that the data for both materials are less than those typically reported for pure SBA-15 mesoporous silicas and PMO materials, respectively.[36,37] This is probably ascribed to the presence of the organic ligand phen in the pore channel, suggesting the organic ligand phen has been successfully grafted into the pore channels of phen-S15 and phen-PMO.[38]

TABLE 1: Structural Parameters[a]

samples	d_{100} (nm)	a_0[b] (nm)	d[c] (nm)	t[d] (nm)	S_{BET} ($cm^2\ g^{-1}$)	V ($cm^3\ g^{-1}$)
phen-S15	9.11	10.52	6.50	4.02	661	1.19
Eu(tta)$_3$phen-S15	11.04	12.74	5.79	6.95	615	1.06
phen-PMO	9.30	10.74	4.65	6.09	837	1.15
Eu(tta)$_3$phen-PMO	11.18	12.91	4.24	8.67	728	1.07

[a] d_{100}, (100) spacing; a_0, cell parameter; d, pore diameter; t, wall thickness; S_{BET}, BET surface area; V, pore volume. [b] Calculated using the equation $a_0 = 2d_{100}/\sqrt{3}$. [c] Pore size distribution by desorption branch (BJH). [d] Calculated by $a_0 - d$.

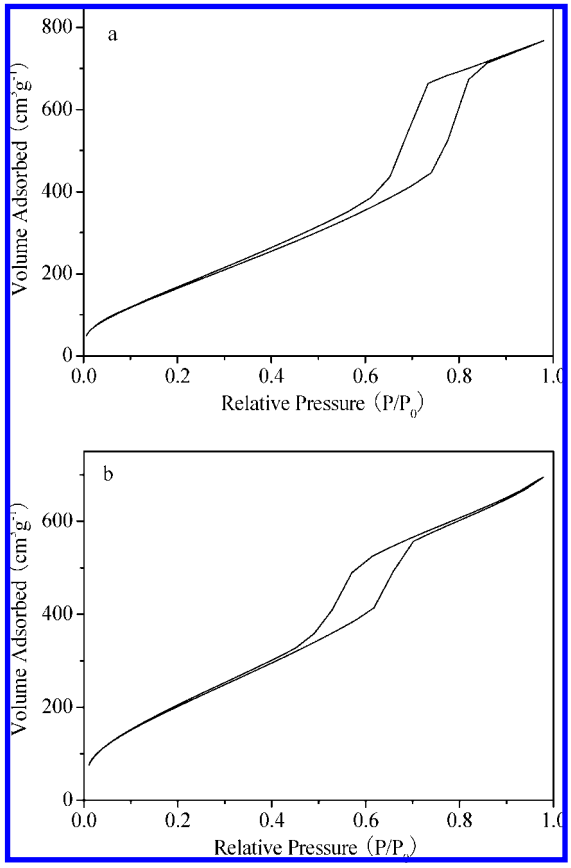

Figure 3. N_2 adsorption−desorption isotherms for surfactant-extracted phen-S15 (a) and phen-PMO (b).

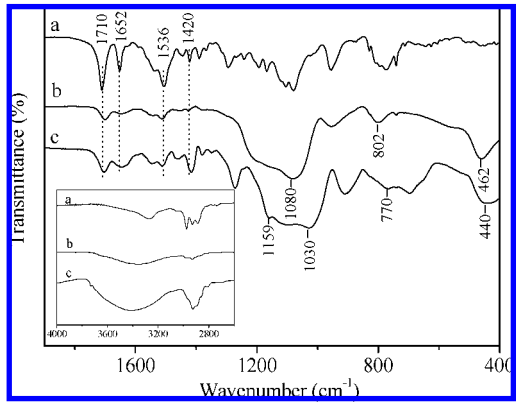

Figure 4. FTIR spectra of phen-Si (a), surfactant-extracted phen-S15 (b), and phen-PMO (c).

The presence and preservation of organic groups in phen-S15 or phen-PMO materials could be proved by the characterization of FTIR. Figure 4 depicts the FTIR spectra of phen-Si (a), surfactant-extracted phen-S15 (b), and surfactant-extracted phen-PMO (c). The formation of Si−O−Si is evidenced by the characteristic bands located at 1030, 1080 cm^{-1} with the shoulder at 1161 cm^{-1} (asymmetric vibrations ν_{as}, Si−O−Si), 802, 770 cm^{-1} (stretching vibrations ν_s, Si−O−Si), and 462, 440 cm^{-1} (in-plane bending vibrations δ, Si−O−Si). A peak at 1413 cm^{-1} is attributed to out-of-plane rocking ω(Si−C). Bands at 1710, 1652, and 1536 cm^{-1}, originating from the −CONH− group of phen-Si, can be observed in both surfactant-extracted materials, which indicates that phen-Si was successfully incorporated into both materials and preserved well after both hydrolysis/condensation reaction and surfactant extraction procedure, consistent with the results of the above nitrogen adsorption−desorption.[39] In addition, compared to the as-synthesized phen-S15 and phen-PMO materials (not shown), the surfactant-extracted phen-S15 and phen-PMO materials only exhibit weak template ν(C−H) vibrations at 2700−3000 cm^{-1} and a disappearance of δ_s(C−H) vibrations at 1375 cm^{-1}, which confirms that most of the surfactant has been removed.[25c]

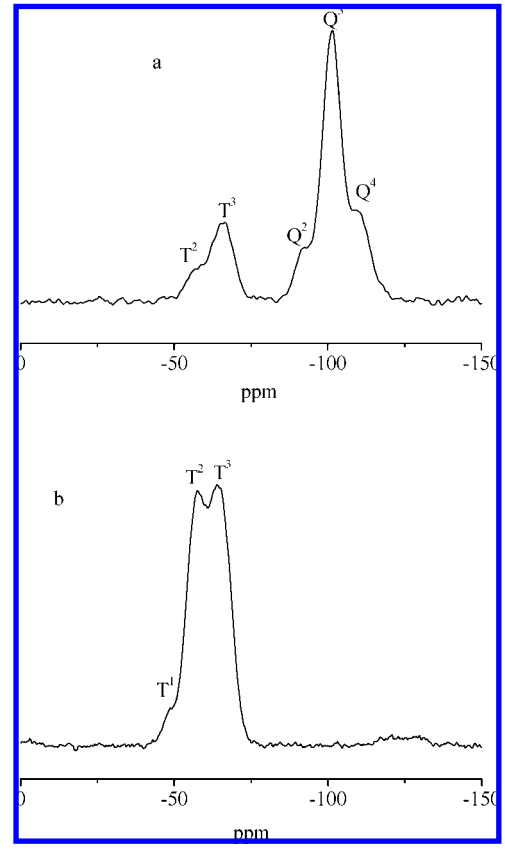

Figure 5. Solid-state^{29}Si MAS NMR spectra of surfactant-extracted phen-S15 (a) and phen-PMO (b).

The solid-state ^{29}Si CP-MAS NMR spectra for surfactant-extracted phen-S15 or phen-PMO materials are presented in Figure 5. In Figure 5a, three resonance peaks at ca. −109.5, −101.5, and −91.8 ppm ascribed to (≡SiO)$_4$**Si** (Q^4), (≡SiO)$_3$**Si**OH (Q^3), and (≡SiO)$_2$**Si**(OH)$_2$ (Q^2), respectively, can be identified clearly. In addition, signals are observed at ca. −66.7 and −56.5 ppm, corresponding to organosiloxane groups

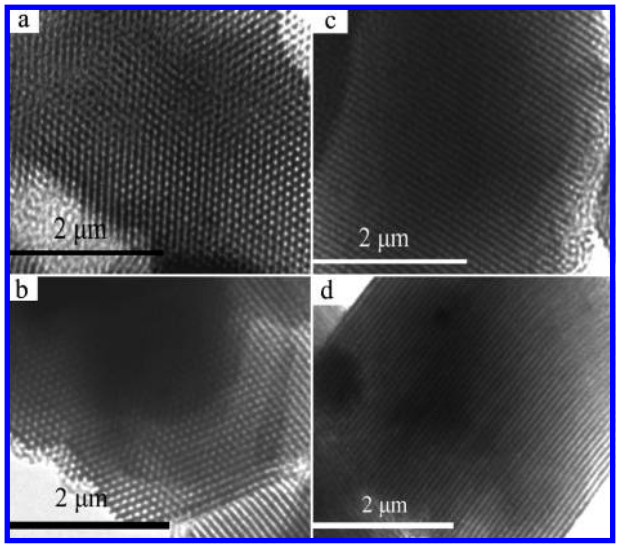

Figure 6. TEM of Eu(tta)$_3$phen-S15 (a, c) and Eu(tta)$_3$phen-PMO (b, d); (a, b) imaged in top view and (c, d) imaged in side view, respectively.

(≡SiO)$_3$**Si**R (T^3) and (≡SiO)$_2$**Si**ROH (T^2), respectively, where R is the organic moiety. The presence of T^2 and T^3 indicates that the organic groups phen-Si have been immobilized to the mesoporous materials, in good agreement with the analysis results of FTIR and N_2 adsorption−desorption. Meanwhile, the relative high intensity of the line at −66.7 ppm indicates that the incorporated phen groups are closely packed on the internal surface of the SBA-15 material via a primary strong linkage (three Si−O−Si covalent bonds). For the sample of phen-PMO, no characteristic peaks of the various siloxane Q^m [Q^m = **Si**(OSi)$_m$(OH)$_{4-m}$, m = 2−4] appear and only resonance organosiloxane peaks attributed to T^n [T^n = R**Si**(OSi)$_n$(OH)$_{3-n}$, n = 1−3] can be seen in the Figure 5b, which confirms that the Si−C bonds of the precursors are stable and do not cleave in the whole synthesis process.

Ternary Complex Eu(tta)$_3$phen Functionalized Mesoporous Silica SBA-15 (Eu(tta)$_3$phen-S15) and Periodic Mesoporous Organosilica (Eu(tta)$_3$phen-PMO) Materials. ***Structural Characterizations.*** The FTIR spectra of Eu(tta)$_3$phen-S15 and Eu(tta)$_3$phen-PMO materials were measured and are shown in the Supporting Information (Figure S1). The appearance of the −CONH− group at 1641 cm^{-1} for two samples demonstrates that the functionalized organic groups phen-Si remain intact after the hydrolysis/condensation reaction, surfactant extraction, and complex-grafting process.

The powder X-ray diffraction analyses of Eu(tta)$_3$phen-S15 (a) and Eu(tta)$_3$phen-PMO (b) are displayed in Figure S2. It can be observed that Eu(tta)$_3$phen-S15 and Eu(tta)$_3$phen-PMO materials still preserve well the typical XRD patterns of SBA-15-type, including a strong (100) reflection at a low angle and two small diffractions ((110) and (200)) at higher angles, indicating that their framework hexagonal orderings have been maintained very well upon the introduction of Eu(tta)$_3$·2H$_2$O. Meanwhile, the hexagonal mesostructures of Eu(tta)$_3$phen-S15 and Eu(tta)$_3$phen-PMO are further confirmed by TEM micrographs (see Figure 6). They both present well the regular hexagonal array of uniform channels, indicating that the mesostructure of the resulting materials can substantially be conserved after the complexation process, coincident with the results of XRD patterns. The distances between the centers of the mesopores for Eu(tta)$_3$phen-S15 and Eu(tta)$_3$phen-PMO are similar and estimated to be about 11 nm, which are in good agreement with the values determined from the corresponding XRD analysis (see Table 1).

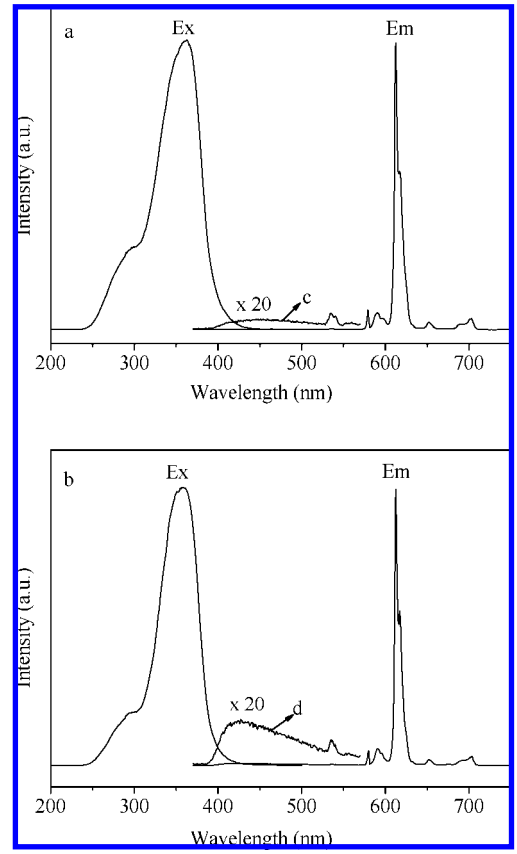

Figure 7. Excitation and emission spectra of Eu(tta)$_3$phen-S15 (a) and Eu(tta)$_3$phen-PMO (b) and the corresponding local magnifications of the emission curves (c) and (d) in solid at room temperature.

The characterization of N2 adsorption−desorption for Eu(tta)$_3$phen-S15 and Eu(tta)$_3$phen-PMO materials further provides proof of the preservation of the mesoporous structure after the introduction of the complex Eu(tta)$_3$·2H$_2$O (see Figure S3). As shown in Figure S3, the typical type-IV isotherms with H^1-type hysteresis loops of mesoporous materials for both samples still remain, similar to those of the corresponding parent materials. The structure parameters of both materials (d, S_{BET}, V, etc.) are summarized in Table 1. It can be observed that the values of d, S_{BET}, and V of Eu(tta)$_3$phen-S15 and Eu(tta)$_3$phen-PMO decrease after introducing the complex Eu(tta)$_3$·2H$_2$O into the relevant phen-S15 and phen-PMO parent materials, which is consistent with the presence of anchored the complex Eu(tta)$_3$·2H$_2$O in the parent mesoporous channels. This phenomenon is due to the dispersion of the complexes Eu(tta)$_3$·2H$_2$O on the surface of the parent materials, resulting in the channels occupied by these complexes.

Photoluminescence Physical Studies. The excitation and emission spectra of Eu(tta)$_3$phen-S15 and Eu(tta)$_3$phen-PMO materials were obtained, respectively, and are shown in Figure 7. The excitation spectra of the resulting hybrid materials Eu(tta)$_3$phen-S15 and Eu(tta)$_3$phen-PMO are similar, which were obtained by monitoring the corresponding emission wavelength of the Eu^{3+} ions at 612 nm. For both spectra, a broad band ranging 200 to 500 nm can be seen, which is ascribed to the $\pi-\pi^*$ electron transition of the ligands. At the same time, it is worth noting that both excitation spectra of the obtained hybrids become narrower than that of Eu(tta)$_3$phen complex,[25c] which may be ascribed to the modification of the organic ligand phen

TABLE 2: Photophysical Data in Solid State[a]

	Eu(tta)$_3$phen-S15	Eu(tta)$_3$phen-PMO
I_{02}	17 227 910	9 519 968
R_I	14.43	14.39
Ω_2 (10^{-20} cm^2)	24.40	24.37
Ω_4 (10^{-20} cm^2)	3.45	3.43
τ (ms)	0.52	0.44
τ_{exp}^{-1}	1923	2273
A_{rad} (s^{-1})	865	860
A_{nrad} (s^{-1})	1058	1413
q (%)	45	38
Φ (%)	22.3	17.5
$n_w/\pm$ 0.1	0.8	1.2

[a] I_{02}, emission intensities of $^5D_0 \rightarrow {}^7F_2$ transition; R_I, intensity ratios of $^5D_0 \rightarrow {}^7F_2$ to $^5D_0 \rightarrow {}^7F_1$; Ω_λ, experimental intensity parameters; τ, decay times; A_{rad}, radiative decay rates; A_{nrad}, nonradiative decay rates; q, emission quantum efficiencies of the $^5D_0$ Eu^{3+} excited state calculated from the decay times and the emission intensities; Φ, absolute emission quantum yields measured at room temperature.

and accordingly to the change of the environment surrounding the europium complex in the mesoporous phen-S15 and phen-PMO materials. In addition, compared to the pure complex Eu(tta)$_3$phen, the maximum excitation wavelengths shift from 392 to 361 and 357 nm, respectively. This pronounced blue-shift of the excitation bands upon the introduction of the europium complex into the phen-S15 and phen-PMO materials is attributed to a hypsochromic effect,[25b−d] which results from the change in polarity of the environment surrounding the europium complex in the hybrids. Furthermore, no f−f transition of Eu^{3+} ion could be detected in the spectra, indicating that the environment of ligands and the part of the host structure affect the energy transfer in Eu(tta)$_3$phen-S15 and Eu(tta)$_3$phen-PMO materials. Upon excitation of the ligands' absorption band at 361 nm, the emission spectrum of Eu(tta)$_3$phen-S15 clearly shows the characteristic emission bands of Eu^{3+} ion centered at 579, 590, 612, 652, and 702 nm, corresponding to the $^5D_0 \rightarrow {}^7F_{0-4}$ transitions, respectively. In the case of Eu(tta)$_3$phen-PMO, the profile of the Eu^{3+} ion emission bands is remarkably similar to that of Eu(tta)$_3$phen-S15. Five characteristic emission bands assigned to the $^5D_0 \rightarrow {}^7F_{0-4}$ transitions are observed, with the $^5D_0 \rightarrow {}^7F_2$ emission as the dominant band. Moreover, two peaks at 535 and 556 nm are observed for two samples, which are attributed to the $^5D_1 \rightarrow {}^7F_1$ and $^5D_1 \rightarrow {}^7F_2$ transitions, respectively. According to the literature reported previously,[25] the luminescent intensities (I_{02}) of the $^5D_0 \rightarrow {}^7F_2$ transition for both materials were calculated and are listed in Table 2. It can be clearly seen that the I_{02} of Eu(tta)$_3$phen-S15 is much higher than that of Eu(tta)$_3$phen-PMO. In addition, it should be noted that, besides the emission lines ascribed to transitions from the $^5D_0$ and $^5D_1$ excited states of Eu^{3+} ions, the emission arising from the host is detected in the range from 400 to 550 nm. As shown in curves c and d in Figure 7, the intensity of the host phen-PMO is higher than that of phen-S15. All above behaviors demonstrate that the ligand-to-Eu^{3+} energy transfer in Eu(tta)$_3$phen-S15 is more efficient than that in Eu(tta)$_3$phen-PMO.

As well-known, the intensity ratio (R_I) of $^5D_0 \rightarrow {}^7F_2$ to $^5D_0 \rightarrow {}^7F_1$ is sensitive to the symmetry around the Eu^{3+} ion and gives valuable information about the chemical microenvironment change of anions coordinating the Eu^{3+} ion.[40] The R_I values for both materials are also listed in Table 2. By comparison, it can be observed that the R_I value for Eu(tta)$_3$phen-S15 is approximately equal to that for Eu(tta)$_3$phen-PMO, which indicates that the symmetries around the Eu^{3+} ion in the hybrid materials are almost the same. However, compared to the R_I value of the pure Eu(tta)$_3$phen,[25c] the R_I values of the above hybrid materials are much higher, which demonstrates that the local symmetries changed upon grafting the complex into matrices and that a more asymmetric environment was occupied by the Eu^{3+} ion, probably due to the effect of confinement.

The luminescence decay times (τ) for Eu(tta)$_3$phen-S15 and Eu(tta)$_3$phen-PMO were measured at room temperature using an excitation wavelength of 355 nm and monitored by the most intense emission line at 612 nm, which are presented in Figure S4. The lifetime profiles for both Eu(tta)$_3$phen-S15 and Eu(tta)$_3$phen-PMO are fitted with single exponentials, demonstrating that all the Eu^{3+} ions locate in the same average local environment in the obtained hybrid materials. The luminescence lifetime was calculated to be 0.52 and 0.44 ms for Eu(tta)$_3$phen-S15 and Eu(tta)$_3$phen-PMO, respectively, which are also listed in Table 2. The shorter lifetime of Eu^{3+} ion in Eu(tta)$_3$phen-PMO indicates that the nonradiative transition probability is higher than that in Eu(tta)$_3$phen-S15.

In order to further discuss the above points, the radiative transition probability (A_{rad}), the nonradiative transition probability (A_{nrad}), and the quantum efficiency, $q = A_{rad}/(A_{rad} + A_{nrad})$, of the $^5D_0$ Eu^{3+} ion excited state were evaluated using a procedure described elsewhere.[41] Meanwhile, the number of water molecules (n_w) coordinated to the Eu^{3+} ions can also be estimated from A_{exp} ($A_{exp} = 1/\tau$) and A_{rad} by the empirical formula $n_w = 1.1(A_{exp} - A_{rad} - 0.31)$. The corresponding data for q and n_w are summarized in Table 2. It can be seen that the quantum efficiencies of Eu(tta)$_3$phen-S15 and Eu(tta)$_3$phen-PMO are higher than that of Eu(tta)$_3$phen,[25c] which may be attributed to the modifications in the Eu^{3+} ion local environment when Eu(tta)$_3$phen is covalently bonded to SBA-15 or PMO materials. In addition, the quantum efficiency of Eu(tta)$_3$phen-PMO (38%) is lower than that of Eu(tta)$_3$phen-S15 (45%), which may be ascribed to the following aspects. First of all, a higher A_{nrad} parameter value occurred in Eu(tta)$_3$phen-PMO than in Eu(tta)$_3$phen-S15; second, compared to Eu(tta)$_3$phen-S15, the small pore diameter of Eu(tta)$_3$phen-PMO has an important effect on the results of the reflection and refraction of the Eu^{3+} ion luminescent center in the channel; and, more importantly, the molecular high-energy vibration of the main flexible framework groups (−CH$_2$−CH$_2$−) in Eu(tta)$_3$phen-PMO results in very strong nonradiative transition. All the above reasons lead to the less efficient intramolecular energy-transfer process (from ligand to Eu(III)) and lower quantum efficiency in Eu(tta)$_3$phen-PMO than in Eu(tta)$_3$phen-S15. But these values are comparable to or much higher than those when Eu complexes with aromatic carboxylic acid ligand[22] or with other β-diketonate ligand[24a] were incorporated into mesoporous silica MCM-41. Moreover, the experimental absolute quantum yields (Φ) of the hybrids are measured, which are presented in Table 2. The absolute emission quantum yields estimated for Eu(tta)$_3$phen-S15 and Eu(tta)$_3$phen-PMO are 22.3% and 17.5%, respectively, well consistent with the above results.

Based on the measurements of the absolute quantum yields, the corresponding chromaticity coordinates (x, y) are also obtained (see Figure 8), which can quantify the emission features. The emission of both hybrids lies in the red spectral region, with coordinates of (0.66, 0.34) for Eu(tta)$_3$phen-S15, and of (0.65, 0.33) for Eu(tta)$_3$phen-PMO. It is noted that these coordinates are equal or very close to those of the well-known standard red phosphor Y_2O_3:Eu (0.66, 0.33).[42]

In addition, the experimental intensity parameters (Ω_λ, λ = 2 and 4) were determined from the emission spectra for Eu^{3+}

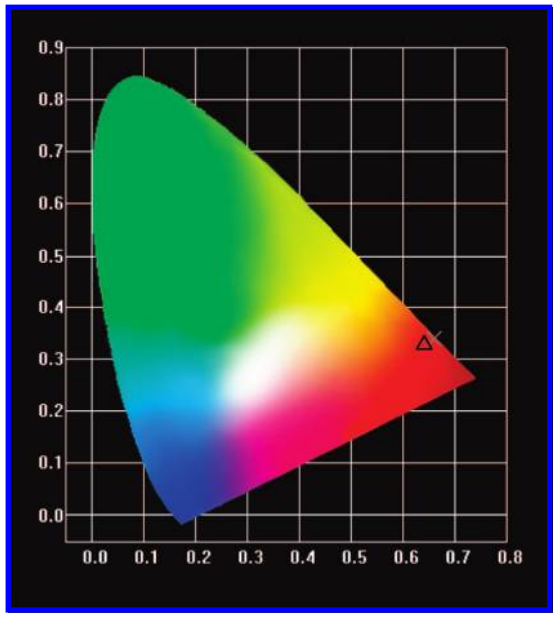

Figure 8. CIE (1931) (*x*, *y*) chromaticity diagram showing the emission color coordinates of Eu(tta)$_3$phen-S15 (×) and Eu(tta)$_3$phen-PMO (△).

ion in Figure 7 based on the $^5D_0 \rightarrow {}^7F_{2,4}$ electronic transitions and the $^5D_0 \rightarrow {}^7F_1$ magnetic dipole allowed transition as the reference,[43−46] and they are estimated by the equation[45]

$$A_{\mathrm{rad}}(J) = \frac{4e^2\omega^3}{3\hbar c^3}\frac{1}{2J+1}\chi\sum_{\lambda}\Omega_\lambda\langle {}^5D_0||U^{(\lambda)}||{}^7F_J\rangle^2$$

where $\lambda = 2$ and 4, e is the electronic charge, ω is the angular frequency of the transition, $\hbar$ is Planck's constant over 2π, c is the velocity of light, χ is the Lorentz local field correction given by $n(n^2 + 2)^2/9$ with the refraction index $n = 1.506$,[43] and $\langle {}^5D_0||U^{(\lambda)}||{}^7F_J\rangle^2$ are the square reduced matrix elements whose values are 0.0032 and 0.0023 for $J = 2$ and 4,[47] respectively. The Ω_6 parameter was not determined since the $^5D_0 \rightarrow {}^7F_6$ transition could not be experimentally observed. Therefore, its influence on the depopulation of the $^5D_0$ excited state is neglected, and the radiative contribution is estimated based only on the relative intensities of the $^5D_0 \rightarrow {}^7F_{0-4}$ transitions. The Ω_2 and Ω_4 intensity parameters for Eu(tta)$_3$phen-S15 and Eu(tta)$_3$phen-PMO are shown in Table 2. It is observed that the values of the Ω_2 intensity parameters for Eu(tta)$_3$phen-S15 and Eu(tta)$_3$phen-PMO are very similar, suggesting the Eu^{3+} ion is in a close chemical environment in both materials, in good agreement with the above lifetime analysis result.

Thermal Stabilities. It is well-known that a good method for investigating and comparing the thermal stabilities of Eu(tta)$_3$phen-S15 and Eu(tta)$_3$phen-PMO is to study their luminescence behavior upon heat treatment. Figure 9 displays the luminescence spectra of both samples after heat treatment in N_2 atmosphere at 400 °C for 2 h, which were obtained upon excitation at 360 nm. It can be observed that after this treatment Eu(tta)$_3$phen-S15 still displays the red emission with the characteristic five strong and sharp lines although accompanying the low emission of the host in the range from 450 to 550 nm. However, for the sample of Eu(tta)$_3$phen-PMO, besides a primary peak at 612 nm, most of the sharp lines for the Eu^{3+} ion characteristic emission are covered by a large and broad emission band centered at 515 nm. This demonstrates that Eu(tta)$_3$phen-S15 has a better thermal stability than Eu(tta)$_3$phen-PMO.

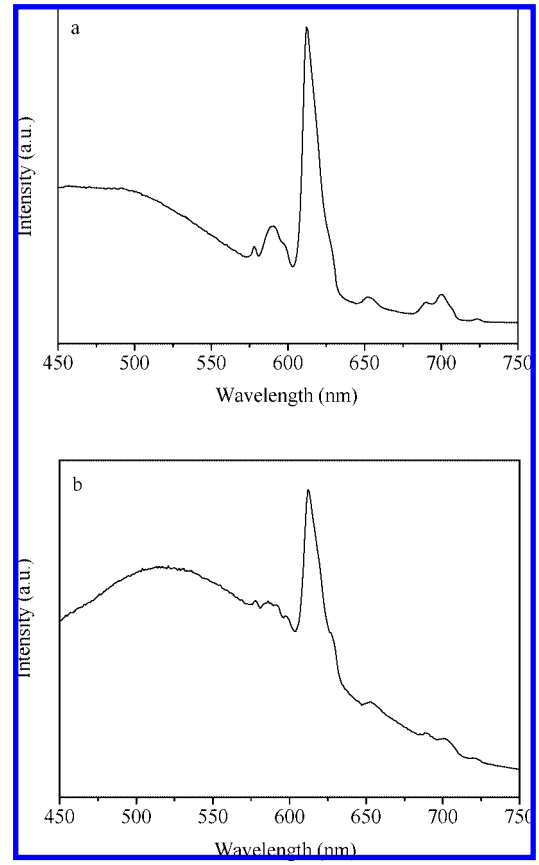

Figure 9. Luminescence spectra recorded after treatment of the samples at 400 °C in N_2 for 2 h. Eu(tta)$_3$phen-S15 (a, $\lambda_{ex} = 360$ nm) and Eu(tta)$_3$phen-PMO (b, $\lambda_{ex} = 360$ nm) measured in solid under ambient conditions.

Conclusions

A novel material Eu(tta)$_3$phen-PMO was synthesized via covalent bonding with ternary lanthanide complex Eu(tta)$_3$phen using a co-condensation method and a ligand exchange reaction. Meanwhile, we also prepared the material Eu(tta)$_3$phen-S15 for comparison. Both hybrid materials were characterized in detail, ranging from structures to properties. The results demonstrate that, compared to the material Eu(tta)$_3$phen-PMO, Eu(tta)$_3$phen-S15 exhibits a more efficient ligand-to-Eu^{3+} energy transfer, stronger emission of Eu^{3+} ion, higher quantum efficiency and yield, longer luminescent decay time, and better thermal stability, suggesting that mesoporous material SBA-15 is a better candidate host for supporting the lanthanide complex than the SBA-15-type PMO material. However, the effect of the microenvironment between the organic complex and two kinds of silica matrix on the luminescence properties still needs further fundamental investigations.

Acknowledgment. This project is financially supported by the National Natural Science Foundation of China (Grant Nos. 20490210, 206301040, and 20602035) and the MOST of China (Grant Nos. 2006CB601103 and 2006DFA42610). L.F. expresses his gratitude to the FCT of Portugal for the financial support of this work.

Supporting Information Available: FTIR spectra, XRD patterns, N_2 adsorption−desorption isotherms, and luminescence decay curves for Eu(tta)$_3$phen-S15 and Eu(tta)$_3$phen-PMO. This material is available free of charge via the Internet at http://pubs.acs.org.

References and Notes

(1) Sammes, P. G.; Yahioglu, G. *Nat. Prod. Rep.* **1996**, *13*, 1.

(2) Okamoto, S.; Vyprachticky, D.; Furuya, H.; Abe, A.; Okamoto, Y. *Macromolecules* **1996**, *29*, 3511.

(3) (a) Iwamuro, M.; Hasegawa, Y.; Wada, Y.; Murakoshi, K.; Kitamura, T.; Nakashima, N.; Yamanaka, T.; Yanagida, S. *Chem. Lett.* **1997**, 1067. (b) Koeppen, C.; Yamada, S.; Jiang, G.; Garito, A. F.; Dalton, L. R. *J. Opt. Soc. Am.* **1997**, *B14*, 155.

(4) Lehn, J. M. *Angew. Chem., Int. Ed. Engl.* **1990**, *29*, 1304.

(5) McGehee, M. D.; Bergstedt, T. B.; Zhang, C.; Saab, A. P.; O'Regan, M. B.; Bazan, G. C.; Srdanov, V. I.; Heeger, A. J. *Adv. Mater.* **1999**, *11*, 1349.

(6) Richardson, F. S. *Chem. Rev.* **1982**, *82*, 541.

(7) Jin, T.; Tsutsumi, S.; Deguchi, Y.; Machida, K.; Adachi, G. *J. Electrochem. Soc.* **1995**, *142*, L195.

(8) Matthews, L. R.; Kobbe, E. T. *Chem. Mater.* **1993**, *5*, 1697.

(9) Embert, F.; Mehdi, A.; Reye, C.; Corriu, R. J. P. *Chem. Mater.* **2001**, *13*, 4542.

(10) Franville, A. C.; Zambon, D.; Mahiou, R.; Troin, Y. *Chem. Mater.* **2000**, *12*, 428.

(11) (a) Binnemans, K.; Lenaerts, P.; Driesen, K.; Görller-Walrand, C. *J. Mater. Chem.* **2004**, *14*, 191. (b) Lenaerts, P.; Storms, A.; Mullens, J.; D'Haen, J.; Görller-Walrand, C.; Binnemans, K.; Driesen, K. *Chem. Mater.* **2005**, *17*, 5194. (c) Driesen, K.; Van Deun, R.; Görller-Walrand, C.; Binnemans, K. *Chem. Mater.* **2004**, *16*, 1531.

(12) (a) de Zea Bermudez, V.; Sá Ferreira, R. A.; Carlos, L. D.; Molina, C.; Dahmouche, K.; Ribeiro, S. J. L. *J. Phys. Chem. B* **2001**, *105*, 3378. (b) Carlos, L. D.; Sá Ferreira, R. A.; Rainho, J. P.; de Zea Bermudez, V. *Adv. Funct. Mater.* **2002**, *12*, 819. (c) Lima, P. P.; Sá Ferreira, R. A.; Freire, R. O.; Almeida Paz, F. A.; Fu, L. S.; Alves, S, Jr.; Carlos, L. D.; Malta, O. L. *Chem. Phys. Chem.* **2006**, *7*, 735.

(13) (a) Li, H. R.; Lin, J.; Zhang, H. J.; Li, H. C.; Fu, L. S.; Meng, Q. G. *Chem. Commun.* **2001**, 1212. (b) Liu, F. Y.; Fu, L. S.; Wang, J.; Meng, Q. G.; Li, H. R.; Guo, J. F.; Zhang, H. J. *New J. Chem.* **2003**, *27*, 233. (c) Li, H. R.; Yu, J. B.; Liu, F. Y.; Zhang, H. J.; Fu, L. S.; Meng, Q. G.; Peng, C. Y.; Lin, J. *New J. Chem.* **2004**, *28*, 1137.

(14) Carlos, L. D.; Videira, A. L. L. *Phys. Rev. B* **1994**, *49*, 11721.

(15) Smirnov, V. A.; Philippova, O. E.; Sukhadolski, G. A.; Khokhlov, A. R. *Macromolecules* **1998**, *31*, 1162.

(16) Bekiari, V.; Pistolis, G.; Lianos, P. *Chem. Mater.* **1999**, *11*, 3189.

(17) Wang, L. H.; Wang, W.; Zhang, W. G.; Kang, E. T.; Huang, W. *Chem. Mater.* **2000**, *12*, 2212.

(18) Yang, C. Y.; Srdanov, V.; Robinson, M. R.; Bazan, G. C.; Heeger, A. J. *Adv. Mater.* **2002**, *14*, 980.

(19) (a) Binnemans, K.; Görller-Walrand, C. *Chem. Rev.* **2002**, *102*, 2303. (b) Van Deun, R.; Moors, D.; De Fré, B.; Binnemans, K. *J. Mater. Chem.* **2003**, *13*, 1520. (c) Arenz, S.; Babai, A.; Binnemans, K.; Driesen, K.; Giernoth, R.; Mudring, A. V.; Nockemann, P. *Chem. Phys. Lett.* **2005**, *402*, 75. (d) Lunstroot, K.; Driesen, K.; Nockemann, P.; Görller-Walrand, C.; Binnemans, K.; Bellayer, S.; Bideau, J. L.; Vioux, A. *Chem. Mater.* **2006**, *18*, 5711.

(20) (a) Xu, Q. H.; Li, L. S.; Liu, X. S.; Xu, R. R. *Chem. Mater.* **2002**, *14*, 549. (b) Xu, Q. H.; Dong, W. J.; Li, H. W.; Li, L. S.; Feng, S. H.; Xu, R. R. *Solid State Sci.* **2003**, *5*, 777.

(21) Bartl, M. H.; Scott, B. J.; Huang, H. C.; Wirnsberger, G.; Popitsch, A.; Chmelka, B. F.; Stucky, G. D. *Chem. Commun.* **2002**, 2474.

(22) Li, Y.; Yan, B. *J. Solid State Chem.* **2008**, *181*, 1032.

(23) Fernandes, A.; Dexpert-Ghys, J.; Gleizes, A.; Galarneau, A.; Brunel, D. *Microporous Mesoporous Mater.* **2005**, *83*, 35.

(24) (a) Gago, S.; Fernandes, J. A.; Rainho, J. P.; Sá Ferreira, R. A.; Pillinger, M.; Valente, A. A.; Santos, T. M.; Carlos, L. D.; Ribeiro-Claro, P. J. A.; Gonçalves, I. S. *Chem. Mater.* **2005**, *17*, 5077. (b) Bruno, S. M; Sá Ferreira, R. A.; Carlos, L. D.; Pillinger, M.; Ribeiro-Claro, P. J. A.; Gonçalves, I. S. *Microporous Mesoporous Mater.* **2008**, *113*, 453.

(25) (a) Li, H. R.; Lin, J.; Fu, L. S.; Guo, J. F.; Meng, Q. G.; Liu, F. Y.; Zhang, H. J. *Microporous Mesoporous Mater.* **2002**, *55*, 103. (b) Meng, Q. G.; Boutinaud, P.; Franville, A.-C.; Zhang, H. J.; Mahiou, R. *Microporous Mesoporous Mater.* **2003**, *65*, 127. (c) Peng, C. Y.; Zhang, H. J.; Yu, J. B.; Meng, Q. G.; Fu, L. S.; Li, H. R.; Sun, L. N.; Guo, X. M. *J. Phys. Chem. B* **2005**, *109*, 15278. (d) Sun, L. N.; Zhang, H. J.; Peng, C. Y.; Yu, J. B.; Meng, Q. G.; Fu, L. S.; Liu, F. Y.; Guo, X. M. *J. Phys. Chem. B* **2006**, *110*, 7249.

(26) (a) Inagaki, S.; Guan, S.; Fukushima, Y.; Ohsuna, T.; Terasaki, O. *J. Am. Chem. Soc.* **1999**, *121*, 9611. (b) Melde, B. J.; Hollande, B. T.; Blanford, C. F.; Stein, A. *Chem. Mater.* **1999**, *11*, 3302. (c) Asefa, T.; MacLachlan, M. J.; Coombs, N.; Ozin, G. A. *Nature* **1999**, *402*, 867.

(27) (a) Burleigh, M. C.; Markowitz, M. A.; Jayasundera, S.; Spector, M. S.; Thomas, C. W.; Gaber, B. P. *J. Phys. Chem. B* **2003**, *107*, 12628. (b) Asefa, T.; Kruk, M.; MacLachlan, M. J.; Coombs, N.; Grondey, H.; Jaroniec, M.; Ozin, G. A. *J. Am. Chem. Soc.* **2001**, *123*, 8520.

(28) (a) Dube, D.; Rat, M.; Beland, F.; Kaliaguine, S. *Microporous Mesoporous Mater.* **2008**, *111*, 596. (b) Vasconcellos-Dias, M.; Nunes, C. D.; Vaz, P. D.; Ferreira, P.; Brandao, P.; Felix, V.; Calhorda, M. J. *J. Catal.* **2008**, *256*, 301.

(29) (a) Nakai, K.; Oumi, Y.; Horie, H.; Sano, T.; Yoshitake, H. *Microporous Mesoporous Mater.* **2007**, *100*, 328. (b) Qiao, S. Z.; Djojoputro, H.; Hu, Q. H.; Lu, G. Q. *Prog. Solid State Chem.* **2006**, *34*, 249.

(30) Langer, R.; Tirrell, D. A. *Nature* **2004**, *428*, 487.

(31) Sanchez, C.; Lebeau, B.; Chaput, F.; Boilot, J. P. *Adv. Mater.* **2003**, *15*, 1969.

(32) Lecomte, J.-P.; Kirsch-De Mesmaeker, A.; Demeunynck, M.; Lhomme, J. *J. Chem. Soc., Faraday Trans.* **1993**, *89*, 3261.

(33) Kloster, G. M.; Watton, S. P. *Inorg. Chim. Acta* **2000**, *297*, 156.

(34) Yang, Q. H.; Liu, J.; Yang, J.; Zhang, L.; Feng, Z. C.; Zhang, J.; Li, C. *Microporous Mesoporous Mater.* **2005**, *77*, 257.

(35) (a) Kresge, C. T.; Leonowicz, M. E.; Roth, W. J.; Vartuli, J. C.; Beck, J. S. *Nature* **1992**, *359*, 710. (b) Beck, J. S.; Vartuli, J. C.; Roth, W. J.; Leonowicz, M. E.; Kresge, C. T.; Schmitt, K. D.; Chu, C. T.-W.; Olson, D. H.; Sheppard, E. W.; McCullen, S. B.; Higgins, J. B.; Schlenker, J. L. *J. Am. Chem. Soc.* **1992**, *114*, 10834.

(36) (a) Zhao, D. Y.; Huo, Q. S.; Feng, J. L.; Chmelka, B. F.; Stucky, G. D. *J. Am. Chem. Soc.* **1998**, *120*, 6024. (b) Zhao, D. Y.; Feng, J. L.; Huo, Q. S.; Melosh, N.; Fredrickson, G. H.; Chmelka, B. F.; Stucky, G. D. *Science* **1998**, *279*, 548.

(37) Muth, O.; Schellbach, C.; Fröba, M. *Chem. Commun.* **2001**, 2032.

(38) Hu, Q. Y.; Hampsey, J. E.; Jiang, N.; Li, C. J.; Lu, Y. F. *Chem. Mater.* **2005**, *17*, 1561.

(39) Li, H. R.; Lin, J.; Zhang, H. J.; Fu, L. S.; Meng, Q. G.; Wang, S. B. *Chem. Mater.* **2002**, *14*, 3651.

(40) Kirby, A. F.; Foster, D.; Richardson, F. S. *Chem. Phys. Lett.* **1983**, *95*, 507.

(41) Supkowski, R. M.; Horrocks, W. D., Jr. *Inorg. Chim. Acta* **2002**, *340*, 44.

(42) Sá Ferreira, R. A.; Karmaoui, M.; Nobre, S. S.; Carlos, L. D.; Pinna, N. *Chem. Phys. Chem.* **2006**, *7*, 2215.

(43) Biju, S.; Ambili Raj, D. B.; Reddy, M. L. P.; Kariuki, B. M. *Inorg. Chem.* **2006**, *45*, 10651.

(44) (a) Malta, O. L.; Couto dos Santos, M. A.; Thompson, L. C.; Ito, N. K. *J. Lumin.* **1996**, *69*, 77. (b) Malta, O. L.; Brito, H. F.; Menezes, J. F. S.; Gonçalves e Silva, F. R.; Alves, S., Jr.; Farias, F. S., Jr.; Andrade, A. V. M. *J. Lumin.* **1997**, *75*, 255.

(45) de Sá, G. F.; Malta, O. L.; de Mello Donegá, C.; Simas, A. M.; Longo, R. L.; Santa-Cruz, P. A.; da Silva, E. F., Jr. *Chem. Rev.* **2000**, *196*, 165.

(46) Teotonio, E. E. S.; Espínola, J. G. P.; Brito, H. F.; Malta, O. L.; Oliveria, S. F.; de Foria, D. L. A.; Izumi, C. M. S. *Polyhedron* **2002**, *21*, 1837.

(47) Carnall, W. T.; Crosswhite, H.; Crosswhite, H. M. *Energy level structure and transition probabilities of the trivalent lanthanides in LaF3*; Argonne National Laboratory: Argonne, IL, 1978.

JP8095488